Talanta 120 (2014) 355–361

Contents lists available at ScienceDirect

Talanta

journal homepage: www.elsevier.com/locate/talanta

Ultrasensitive electrochemical detection of cancer associated biomarker HER3 based on anti-HER3 biosensor

Münteha Nur Sonuç [a], Mustafa Kemal Sezgintürk [b,*]

[a] Namık Kemal University, School of Health, Nutrition and Dietetics Department, Tekirdağ, Turkey
[b] Namık Kemal University, Faculty of Science and Arts, Chemistry Department, Biochemistry Division, Tekirdağ, Turkey

ARTICLE INFO

Article history:
Received 27 July 2013
Received in revised form
27 November 2013
Accepted 30 November 2013
Available online 19 December 2013

Keywords:
HER3
Anti-HER3
Biosensor
Electrochemical impedance spectroscopy
Cancer biomarker

ABSTRACT

The development of a new impedimetric biosensor for the detection of HER3, based on self-assembled monolayers (SAMs) of 4-aminothiophenol on gold electrodes, is reported. Anti-HER3 was used as a biorecognition element for the first time in an impedimetric biosensor. Cyclic voltammetry (CV) and electrochemical impedance spectroscopy (EIS) techniques were applied to characterize the immobilization process and to detect HER3. To provide the best biosensor response all experimental parameters were optimized. In addition, Kramers–Kronigs transform was also performed on the immobilization and measurement processes successfully. The biosensor had a linear detection range of 0.4–2.4 pg/mL. The chrono-impedance technique to real time monitor the interaction between HER3 and anti-HER3 is also implemented. The biosensor has exhibited good repeatability and reproducibility. To demonstrate the feasibility of the biosensor in practical analysis, the artificial serum samples were experienced.

1. Introduction

The human epidermal growth factor receptor family (HER) consists of four homologous members: EGFR (epidermal growth factor receptor, HER-1 or c-*erb*B-1), HER-2 for which no ligand has been described by now, HER3, and (HER-4). [1] These transmembrane glycoproteins have an extracellular ligand binding domain, a transmembrane region, and an intracellular domain with tyrosine kinase activity [2] though HER3 has little or no tyrosine kinase activity and this is the most distinct difference between it and the other family members [3]. As etiological members of HER family have been related to the progression of some type of human cancers through overexpression or mutational activation, including cancers of the breast, lung, head and neck, brain, and skin [4–6]. HER3 has been shown to be highly expressed in melanomas [6–8], some prostate cancers [9], colorectal cancers [10–14], breast cancers [15–17], ovarian tumors [18], and notably childhood glioma [6,19]. Moreover recent evidence indicated that HER3 responsible for tumor resistance to therapeutic agents targeting EGFR or HER-2 has illuminated its critical role in cancer [20]. Therefore there are interests which have recently been occured by the possibility of utilizing the HER3 as prognostic indicators in some type of carcinomas. Normal physiological levels of HER3 in a person range from 0.06 ng/mL to 2.55 ng/mL. However, in a pathological case, the abnormal values of HER3 should be increased up to 12 ng/mL [21]. Characterizations of HER3 were carried out by immunohistochemistry [2,22], Southern blot [23], enzyme linked immuno assay (ELISA) [24,25], Northern blot [26] for detection of expressed HER3 in blood or tissues. Recently, an electrochemical strategy based on aptamers and nanoprobes was developed for the rapid detection of HER-3 [27]. In the reported study a nanoprobe consisting of aptamers and DNA capped nanocrystals has been designed for the electrochemical detection of HER3.

Affinity-binding based impedimetric biosensors become an efficient method since they are speed, direct and label-free electrochemical immunosensors [28] and due to their affordability and availability, a trend towards the development of impedimetric biosensors appears to be underway. The application of immunosensors for the detection of a wide range of analytes in clinical diagnostics and environmental control is well established. The improvement of hand held devices for point of care detection hold promising and attractive alternatives to existing laboratory-based immunochemical assays [29].

Aim of this study is development of a new impedimetric biosensor, based on the use of anti-HER3 for the determination of HER3 by forming a self-assembled monolayer on gold electrodes. anti-HER3 immobilization steps and measurements were evaluated by cylic voltammetry and electrochemical impedance spectroscopy. In order to investigate interaction betwwen HER3 and anti-HER3 immobilized onto gold surface, a novel impedimetric method called single frequency impedance measurement is also presented.

* Corresponding author. Tel.: +90 282 250 26 05.
E-mail addresses: msezginturk@hotmail.com, msezginturk@nku.edu.tr (M.K. Sezgintürk).

0039-9140/$ - see front matter © 2013 Elsevier B.V. All rights reserved.
http://dx.doi.org/10.1016/j.talanta.2013.11.090

2. Materials and methods

2.1. Materials

All reagents were obtained from Sigma-Aldrich (St. Louis, MO, USA). HER3, (human epidermal growth factor receptor family-3) and anti- HER3 were also purchased from Sigma-Aldrich. HER3, anti-HER3, and 0.1% BSA (bovine serum albumin) were prepared in 50 mM, pH 7, phosphate buffer and further dilutions were made using sterile phosphate buffer (pH 7.0, 0.01 M) as well. HER3 and anti-HER3 portions were prepared at certain concentrations and were stored at −20 °C until use. Synthetic serum solution was prepared by using 4.5 mM KCl, 5 mM CaCl2, 1.6 mM MgCl2, 4.7 mM (D+)-glucose, 2.5 mM urea, 0.1% human serum albumin, and 145 mM NaCl. A redox probe solution was prepared in 50 mM, pH 7.0, phosphate buffer which contained 0.1 M KCl, 5 mM $Fe(CN)_6^{4-}$ and 5 mM $Fe(CN)_6^{3-}$.

Gold working electrodes (1.6 mm^2 surface area), Ag/AgCl reference electrode, and Pt counter electrode were obtained from BASi (Warwickshire, UK). Electrochemical experiments were carried out by using a Compactstat with integrated impedance analyzer (Ivium Technologies, Eindhoven, The Netherlands) and Gamry Potentiostate/Galvanostate, Reference 600 (Gamry Instruments, Warminster, USA) interfaced with a PC. All electrochemical experiments were carried out in a Faraday cage (from iBAS, Warwickshire, UK) to block out external static electric fields.

3. Methods

3.1. Preparation of the self-assembled monolayer of 4-aminothiophenol

Before the use the gold electrodes were first polished with 0.05 μm alumina powder and then washed with ultrapure water. Following that, the electrodes were ultrasonically washed in absolute ethanol for 2 min to remove alumina residues. Then the electrodes were immersed in Piranha (H_2O_2/H_2SO_4, 30/70, v/v) solution for 3 min. Following that the electrodes were washed with ultra pure water. For the next step, the surfaces of the electrodes were dried by a pure argon stream. This polishing and cleaning procedure was repeated before every electrode preparation step. The clean gold electrodes were immediately immersed into 4-aminothiophenol solution (0.1 M, in pure ethanol) for 16 h. After this period, they were rinsed with ethanol and gently dried with an argon stream.

3.2. Anti-HER3 immobilization procedure on SAM of 4-ATP

For anti-HER3 immobilization, the electrodes modified with 4-ATP (Au/4-ATP) were immersed into 2.5% glutaraldehyde solution for 15 min in a dark surrounding to activate the amino ends of the 4-aminothiophenol. Later, the gold electrodes were washed with ultra-pure water gently, and were then dried by a pure argon stream again. Then 10 μl of anti-HER3 portion was applied to the active electrodes surface by a pipette. The electrodes were allowed to incubate for an hour in moisture and dark medium. After that electrodes were washed and dried as noted above. Finally 10 μl BSA solution (0.1%) was dropped onto the electrodes to block the active ends on the surface. The bare electrodes and the modified electrodes were indicated as Au, Au/4ATP, Au/4ATP/anti-HER3, and Au/4ATP/anti-HER3/BSA.

3.3. Measurement procedure

Cyclic voltammetry was used to characterize the layer-by-layer formation of the biosensors. The potential was varied between 0 and 500 mV (step size, 20 mV; scan rate, 50 mV/s) in the presence of 5 mM $K_3[Fe(CN)_6]/K_4[Fe(CN)_6]$ (1/1) solution, which served as a redox probe containing 0.1 M KCl. For electrochemical impedance studies, an alternating wave with 10 mV of amplitude was applied to the electrode over the formal potential of the redox couple (0.18 V). The redox couple used for impedance studies was the same as that used in cyclic voltammetry. Impedance spectra were collected in the frequency range between 10000 and 0.05 Hz.

After each of the anti-HER3 biosensors was assembled, the biosensor surface was used to interact with the HER3 solution. The standard solution of HER3 was injected over the biosensor surface by a micropipette. For each time measurement, the injection volume was 5 μL. The response value was read after one hour incubation in a moisture and dark medium. After this incubation period, the biosensor was gently immersed into the ultrapure water 20 times to remove physically adsorbed HER3 molecules. Finally, the biosensor was again put into the cell containing the $Fe(CN)_6^{4-/3-}$ redox probe solution and the electrochemical measurements were carried out as described previously.

4. Results and discussion

4.1. Anti-HER3 immobilization by SAM of 4-aminothiophenol

The use of SAMs has shown to provide molecular level control over the immobilization of several types of biomolecules [30].

Formation of organized monolayers of alkanethiols on gold surfaces was first discovered by Nuzzo and Allara [31]. Since then SAMs have been widely used in many different applications for surface modifications. SAMs can also be integrated with several molecular and cellular processes such as protein interactions [32,33]. Moreover they have been used for constructing molecular switching [34,35], biosensors [36–38] and micro/macrroarrays [39,40]. In fact the success of SAMs in several technological fields is caused by important advantages of gold itself. For example; gold is an inert metal, consequently oxidation could not easily occured on gold surfaces. Moreover the gold–sulfur interaction is a strong and a specific chemical process that allows the formation of self-assembled monolayers carrying other functional groups. Most importantly preparation of SAMs is a quite simple process which does not require sophisticated and high-priced equipment or extensive experience to be performed successfully.

This is the first biosensor system for determination of HER3 by SAMs modified gold electrode and using anti-HER3 as a biorecognition component. The changes occured on the surfaces of modified gold electrodes by formation of SAM and anti-HER3 immobization were investigated using CV and EIS. In the experiments, the redox couple $Fe(CN)_6^{3-/4-}$ was preferred for use as an electrochemical probe because $Fe(CN)_6^{3-/4-}$ was more sensitive to surface modifications, such as binding of HER3 to its antibody. Electrochemical impedance spectra were significantly affected by modifications on the electrode surface. Electrochemical impedance spectroscopy consists resistive and capacitive elements besides Warburg element and is a powerful method for analyzing the complex electrical resistance of a system. EIS is also sensitive to surface characteristic and changes of bulk properties, moreover it is especially well-suited to the detection of binding events on the transducer surface in biosensor fields, therefore it is a valuable and progressive technique [41].

A well-defined characteristic voltammogram of the redox couple could be observed on the bare gold electrode (Fig. 1A).

Firstly, thiol group in 4-ATP allowed the assembly on Au electrode through sulfur–Au interaction. It was obvious that the anodic and cathodic peak currents did not considerably change after self-assembly organization of 4-ATP on the gold electrode surface. Probably the self-assembled monolayer of 4-ATP resulted in a slight increase in electron transfer due to its positively charged amino ends which could attract the negatively charged redox probe. Moreover, benzene ring of 4-ATP should presumably reduce the molecular flexibility of the monolayer. Besides this benzene ring provides higher electrical conductivity due to possessing high density of delocalized electrons in its structure.

As known 4-ATP is a conjugated molecule which is a system of connected p-orbitals with delocalized electrons in compounds with alternating single and multiple bonds, which in general may lower the overall energy of the molecule and increase stability. Consequently 4-ATP should promote electron transfer through the electrode surface.

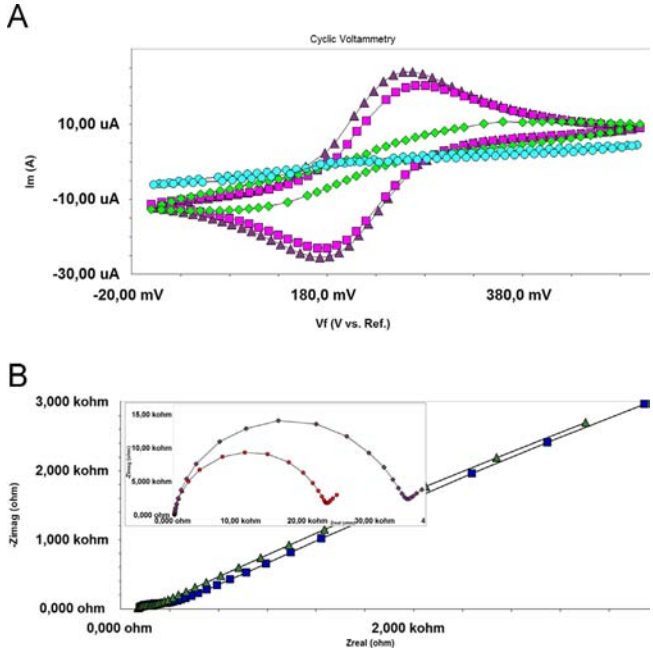

Fig. 1. **(A)** Cyclic voltammograms of anti-HER3 immobilization by covalent attachment **(B)** Electrochemical impedance spectra of anti-HER3 immobilization steps [-▲-▲-:Au/bare, -■-■-: Au/4-ATP, -◆-◆-: Au/4-ATP/anti HER3, -●-●-:Au/4-ATP/anti HER3/BSA].

Then the next step was the glutaraldehyde activation of terminal $-NH_2$ groups of 4-ATP SAMs, then immobilization of anti-HER3 the peak current decreased considerably compared to that obtained at an Au/4-ATP.

The impedance changes of the modified gold electrode are shown in Fig. 1B. The complex impedance is displayed as the sum of the real and imaginary components (Zre and Zim). As can be seen from Fig. 1B, after the 4-ATP monolayer was self-assembled on the electrode, the interfacial electron transfer resistance, R_{ct}, was almost the same as that of the bare gold electrode. When the 4-ATP modified electrode was further modified with the glutaraldehyde which was a crosslinker agent, and after anti-HER3 molecules were attached to the modified electrode, the charge transfer resistance was significantly increased in comparison with the previously modified electrode surfaces. This increase showed the successful immobilization of anti-HER3 on the gold electrode modified with 4-aminothiophenol. In the last step of immobilization of anti-HER3, the electrode surface was modified with bovine serum albumin to block free active ends. As expected, this caused a further increase in R_{ct}. The results obtained for the immobilization steps showed agreement between cyclic voltammograms and electrochemical impedance spectra. It can be concluded that there was a good linear relationship between semicircle diameters and electrode layers which indicated successively construction of the biosensor. A schematic representation is given in Scheme 1.

4.2. Optimization experiments of anti-HER3 biosensor

The fabrication steps of the anti-HER3 based biosensor were examined in terms of the concentration of 4-ATP for SAM formation, glutaraldehyde percentage for crosslinking, and anti-HER3 and HER3 incubation periods for effective binding processes.

Firstly, the self-assembled monolayers (SAMs) of 4-aminothiophenol on gold electrode surface provided a good substrate for attachment of anti-HER3 easily. The experiments showed that the response of the biosensor would be influenced by the concentrations of 4-ATP. In order to clarify the effect of 4-ATP concentration on the biosensor performance, 4-ATP solutions with different concentrations such as 5, 10, 50 and 100 mM were utilized for biosensor fabrication. The results showed that the performance of anti-HER3 immobilization was affected by concentration of 4-ATP. R_{ct} values were determined as 429.9, 693.1, 436.8, 188 Ω. It can be seen from EIS results, SAM of 100 mM 4-ATP has showed minimum blocking effect as expected from 4-ATP. Consequently, 100 mM was chosen for further studies.

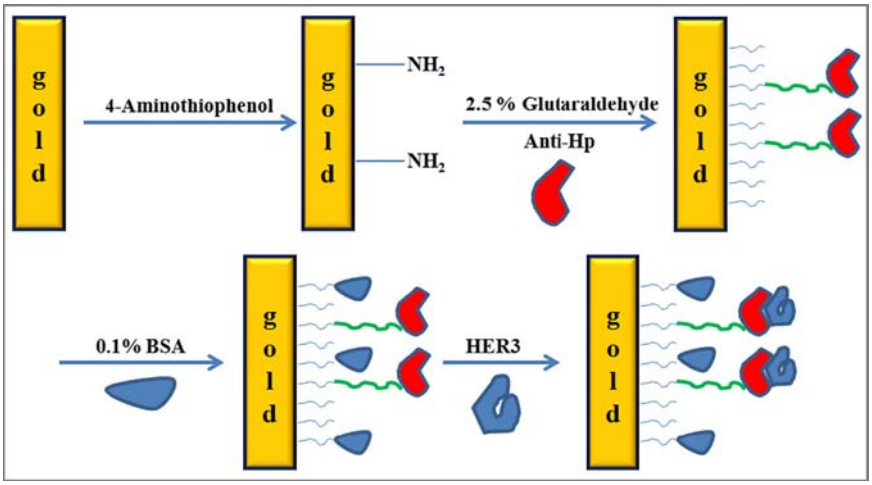

Scheme 1. Representation of immobilization steps of anti-HER3 onto Au electrode.

The behavior of the biosensor was studied against different glutaraldehyde concentrations 0.5%, 1.0%, 2.5%, 3.5%, and 5.0%. R_{ct} values were determined as 6990, 11200, 22700, 20800, 32700 Ω, respectively. The highest R_{ct} value was obtained with the biosensor constructed by glutaraldehyde 5%. However as an optimum glutaraldehyde concentration 2.5% was chosen for further studies. This is why high glutaraldehyde concentrations should probably cause to denature anti-HER3.

The next step in the optimization studies was concentration of anti-HER3 needed for effectively binding of HER3. For this purpose, 0.02 μg μl^{-1}, 0.2 μg μl^{-1}, 5 μg μl^{-1}, 10 μg μl^{-1}, 15 μg μl^{-1}, and 20 μg μl^{-1} anti-HER3 concentrations were used for the construction of corresponding biosensors. The experiment results showed that the biosensor performance was strictly dependent on the concentration of anti-HER3 used in the immobilization. R_{ct} values for different anti-HER3 amounts (0.02 μg μl^{-1}, 0.2 μg μl^{-1}, 5 μg μl^{-1}, and 10 μg μl^{-1}) were determined as 4930, 4270, 4220, and 5740 Ω, respectively. However the biosensors prepared with anti-HER3 solutions of 15 μg μl^{-1} and 20 μg μl^{-1} have not showed good immobilization performance and could not subtract an impidimetric value. As can be seen from the cyclic voltammograms, (Fig. 2A) an increase in anti-HER3 concentration resulted in decrease in anodic and cathodic peak currents. From Fig. 2B, it can be seen that increasing the concentration of anti-HER3 increased the interfacial electron transfer resistance compared with the lower concentrations of anti-HER3. This was because of the more effective blocking behavior of anti-HER3 toward electron transfer. As a result, in further biosensors anti-HER3 concentration was chosen as 10 μg μl^{-1} for optimum performance.

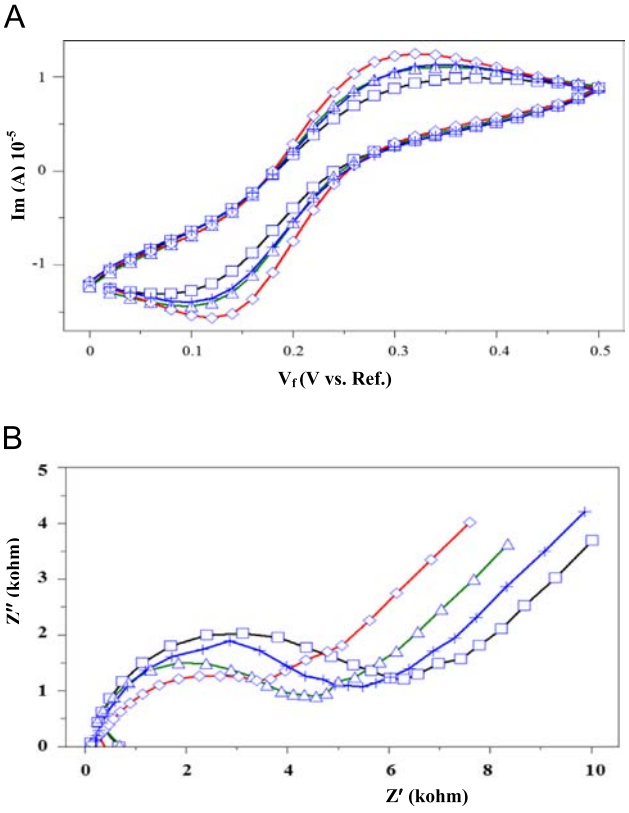

Fig. 2. Evaluation of the effect of anti-HER3 incubation concentration on the biosensor response. (A) Cyclic voltammograms related different incubation concentrations, and (B) electrochemical impedance spectra obtained for different anti HER3 incubation concentrations [-◆-◆-: 0.02 μg μL^{-1}, -▲-▲-: 0.2 μg μL^{-1} -+- +: 5 μg μL^{-1}, -■-■-: 10 μg μL^{-1}].

4.3. Analytical characteristics of anti-HER3 biosensor

In this study, electrochemical impedance spectroscopy was used to determine the amount of redox probe associated with changes in the electron transfer resistance at the anti-HER3 biosensor surface. The charge transfer resistances related with the HER3 concentrations were calculated by the potentiostate system software.

To obtain a calibration curve for HER3 the charge transfer resistance differences related to different HER3 amounts were calculated by the following equation:

$$\Delta R_{ct} = R_{ct(anti-HER3/BSA/HER3)} - R_{ct(antiHER3/BSA)}$$

where $R_{ct(anti\text{-}HER3/BSA/HER3)}$ is the value of the charge transfer resistance after anti-HER3 is coupled to HER3, while $R_{ct(antiHER3/BSA)}$ is the value of the charge transfer resistance when anti-HER3 is immobilized on the electrode and the bovine serum albumin to block active ends. It can be seen from Fig. 3A, CV peak currents decreased with an increase in the concentrations of HER3 standard solutions. Fig. 3B shows the Nyquist plots evaluation of the biosensor for different HER3 concentrations. It was observed that the semicircle diameter in the Nyquist plots increased with increasing HER3 concentration.

Moreover, the impedance spectra should be fitted with an equivalent circuit model as shown in Fig. 4 where the capacitance C_{dl} is the double-layer capacitance, R_{ct} is the charge transfer resistance in low frequency, Z_w is the Warburg element, and R_s is the resistance of the electrolyte and all the connections.

The rise of HER3 concentration increased the charge transfer resistance, R_{ct}, achieving a linear range between 0.4 and 2.4 pg/mL. A calibration graph for HER3 was prepared with the help of the differences in charge transfer resistances after HER3 binding. The calibration curve is given in Fig. 5 and the results are given Table 1.

Shaoping and coworkers reported in the published paper that anti-HER3 antibodies showed a linear relation in the range of 0.2–1.0 fmol HER3 [26]. However all steps of the fabrication of nanoprobes included extremely time-consuming procedures and expensive materials. ELISA is the most frequently used in vitro

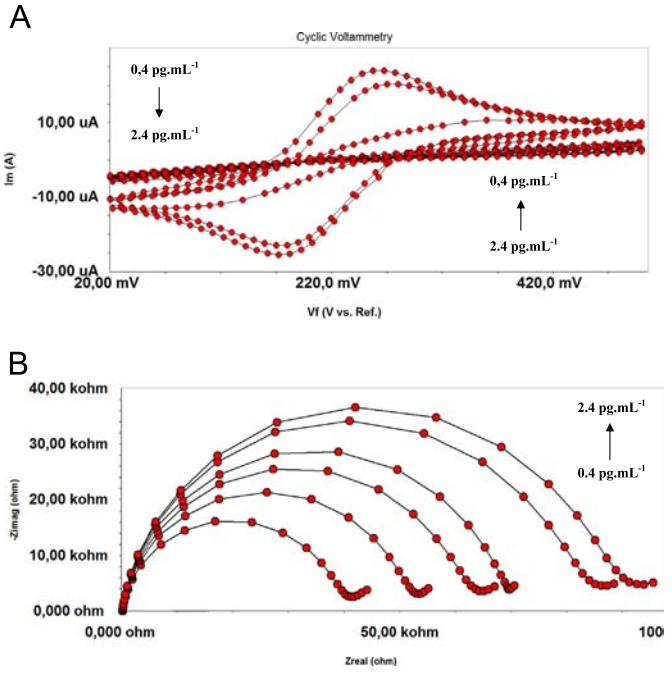

Fig. 3. Cyclic voltammograms (A) and impedance spectrums (B) obtained for different concentrations of HER3.

enzyme-linked immunosorbent assay for the quantitative measurement of HER3 in the literature. This assay employs an antibody specific for HER3. The detectable limit of this method was reported as less than 4 pg/mL [24]. However ELISA method also required several time consuming steps. The immobilization of the biosensor presented here required simple operations. Moreover anti-HER3 was economically immobilized onto gold electrodes. Beside the biosensor revealed a good linear detection range from 0.4 pg/mL to 2.4 pg/mL which was better than the other reported methods.

In this study, Kramers–Kronig transform was one of the most important parameters analyzed. The Kramers–Kronig relations

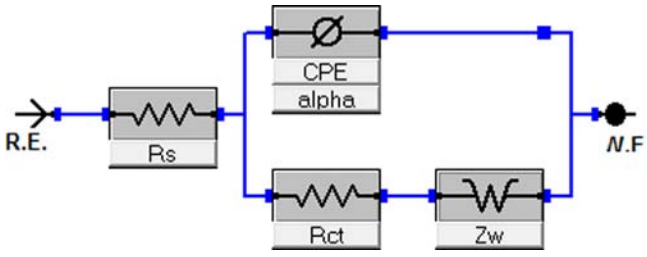

Fig. 4. Equivalent circuit model applied to fit the impedance measurements.

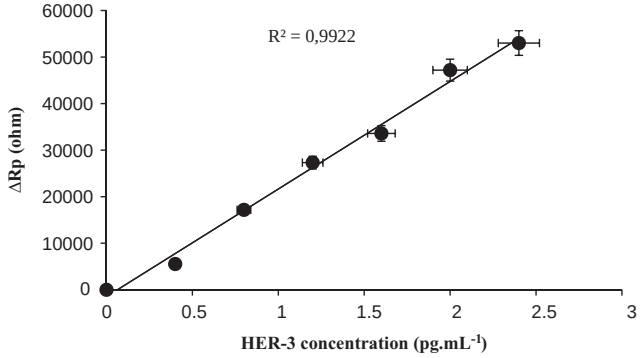

Fig. 5. HER3 calibration curve obtained at optimal working conditions.

are integral equations that constrain the real and imaginary components of complex quantities for systems that satisfy conditions of linearity, causality, and stability [42,43] In principle, the Kramers–Kronig relations can be used to determine whether the impedance spectrum of a given system has been influenced by bias errors caused, for example, by instrumental artefacts or time-dependent phenomena. This information is critical to the analysis and interpretation of electrochemical impedance spectroscopy data due to difficulties with their applications. The Kramers–Kronig relations have been applied to electrochemical systems by direct integration of the equations, by experimental observation of stability and linearity, by regression of specific electrical circuit models, and by regression of generalized measurement models [44,45]. Direct integration of the Kramers–Kronig relations involves calculating one component of the impedance from the other, e.g., the real component of impedance from the measured imaginary component. The result is compared to the experimental values obtained.

In the presented study, Kramers–Kronig transforms were performed by the software called GamryEchemAnalyst (Ver. 5.61). Goodness of fit values are given in Table 1. The plots of Kramers-Kronig transforms performed on different layers of biosensor surfaces are shown Fig. 6.

In order to evaluate the sensitivity of the biosensor the limit of detection (LOD) is one of the most important parameters to be determined. The limit of detection or detection limit, which was the lowest HER3 amount that could be determined to be statistical by the resulting biosensor, was calculated as 0.28 pg/mL ($[k\ S_{blank}/m]$, $k \sim 3$, S_{blank} and m represent impedance signal obtained for blank sample and the slope, respectively). Beside, a limit of quantitation (LOQ), which meant the lower limit of quantitation was also calculated as 0.94 pg/mL ($[k\ S_{blank}/m]$, $k \sim 10$, S_{blank} and m represent similar magnitudes with LOD). It can be concluded that the biosensor based on anti-HER3 could analyze HER3 sensitively.

An effective electrochemical impedimetric method was also performed on biosensor system for the first time. Electrochemical Impedance Spectroscopy (EIS) has been widely used in the last decades as an important electrochemical method to investigate the surface modifications, immobilization performances of any biomolecules etc. Moreover it is utilized to calculate the charge transfer

Table 1
The results for Kramers–Kronig transforms, reproducibility, and the sample analysis.

Kramers–Kronig transforms for different layers of gold layer based biosensor			
Biosensor surfaces			Goodness of fit values
Bare Au			2.90E−04
Au/4ATP			9.01E−07
Au/4ATP/antiHER3			7.53E−05
Au/4ATP/antiHER3-BSA			3.42E−05
Au/4ATP/antiHER3/BSA/HER3			2.79E−05
Reproducibility of the biosensor			
Biosensor numbers	R^2	y	Linear ranges (pg/mL)
1	0.9804	$1958.5x-2375.9$	0.4–2.4
2	0.9903	$2816.1x-2415.7$	0.4–2.4
3	0.9922	$9241.1x-10704$	0.4–2.4
4	0.9818	$4383.2x-5910$	0.4–2.4
5	0.9895	$1757.7x-1682$	0.4–2.4
6	0.9912	$3837.7x-2643.6$	0.4–2.4
7	0.991	$4387.1x-3164$	0.4–2.4
VEGF detection in artificial serum samples			
VEGF (pg/mL)			
Added	Found by the biosensor	% Recovery difference	% Relative
0.4	0.416	104	4
1.2	1.225	102.1	2.1

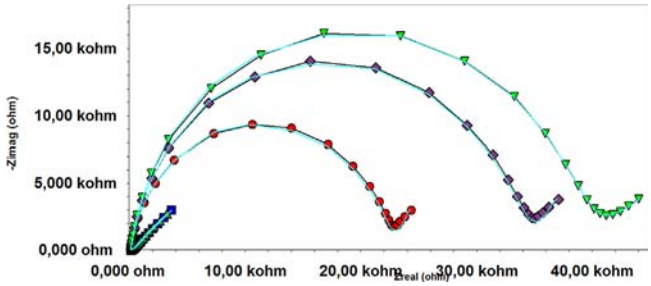

Fig. 6. The plots of Kramers–Kronig transforms performed on different layers of biosensor surfaces. The turquoise lines show the Kramers–Kronig transforms performed and fitted on the experimental data and the red lines show experimental results. -▲-▲-: Au/bare, -■-■-: Au/4-ATP, -●-●-:Au/4-ATP/anti HER3, -◆-◆-: Au/4-ATP/antiHER3/BSA, -▼-▼-: Au/4-ATP/anti HER3/BSA/HER3. (For interpretation of the references to color in this figure legend, the reader is referred to the web version of this article.)

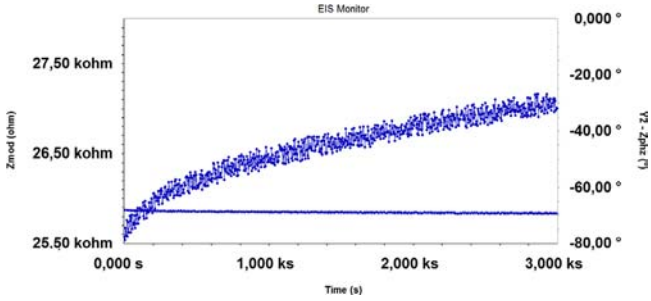

Fig. 7. Single frequency impedance measurement for the interaction between Anti-HER3 and HER3

resistances of a modified surface. In this study one of the most important goals was to characterize the interaction between HER3 and anti-HER3 by using novel technique "single frequency impedance". This technique measures the impedance at a fixed frequency versus time. In this way it should be possible to control the experiment with a repeat time and a total time. For this purpose the potentiostate was setup at a fixed frequency, as 20 Hz. The impedance was monitored at this fixed frequency as a function of time and phase angle during 60 min. The result can be shown in Fig. 7.

Fig. 7 showed that the results of single frequency impedance measurements should be extremely convenient for the evaluation and characterization of a biosensor. Moreover this novel technique should be used to clarify slow time-dependent changes occurred on the biosensor surface. Otherwise the experiments showed that single frequency impedance could give very important information on binding kinetics of an antibody and antigen.

The storage stability of the resulting biosensor was checked during a period of about 15 days. For this purpose the biosensors were stored under dry conditions at 4 °C during different storage periods. A relatively good stability was obtained for approximately 10 days, after which the the impedance value obtained for application of 0.4 pg/mL of HER3 started to decrease. The sensitivity of the biosensor decreased only by about 6% from the initial value after 10 days, which meant that anti-HER3 was well immoblized on the gold electrode surface. After 2 weeks of storage periods, biosensor performance decreased by 16.3%, which meant that partial denaturation of the protein structure of anti-HER3 caused by storage periods longer than 10 days.

Eventually, to demonstrate the feasibility of the biosensor in practical analysis, the artificial serum samples were prepared by the addition of HER3 standard solutions. These artificial serum samples were analyzed using the proposed impedimetric biosensor based on anti-HER3 as shown in Table 1.

5. Conclusion

In conclusion, we have successfully developed a novel, efficient and simple constructed biosensor utilizing anti-HER3 as a bior-ecognition element for the diagnosis of HER3. In the literature, anti-HER3 was used for the first time for construction of an impedimetric biosensor. Optimized experimental conditions for the fabrication and operation of the biosensor were investigated. Moreover, the Kramers–Kronig transforms were applied to the biosensor system. These transforms showed that the impedance data obtained by the biosensor was stable, linear, and causal. Under optimal conditions the biosensor based on anti-HER3 exhibited a determination range from 0.4 pg/mL to 2.4 pg/mL. The impedimetric biosensor also displayed excellent repeatability and reproducibility. As can be seen from the results of artificial serum sample analyses the biosensor proposed here could be a good alternative to other detection methods for HER3 in clinical analysis.

Acknowledgment

Support from TÜBİTAK (The Scientific and Technological Research Council of Turkey, Project number: 109 T 172) is greatly acknowledged.

References

[1] A.K. Koutras, T.R. Jeffry Evans, Onco Targets Ther. 1 (2008) 5–19.
[2] R. Srinivasan, E. Benton, F. McCormick, H. Thomas, W.J. Gullick, Clin. Cancer Res. 5 (1999) 2877–2883.
[3] M.X. Sliwkowski, G. Schaefer, R.W. Akita, J.A. Lofgren, V.D. Fitzpatrick, A. Nuijens, B.M. Fendly, R.A. Cerione, R.L. Vandlen, K.L. Carraway, J. Biol. Chem. 269 (1994) 14661–14665.
[4] T.Y. Kew, J.A. Bell, S.E. Pinder, H. Denley, R. Srinivasan, W.J. Gullick, R.I. Nicholson, R.W. Blamey, I.O. Ellis, Br. J. Cancer 82 (2000) 1163–1170.
[5] A.V. Koutsopoulosa, D. Mavroudis, K.I. Dambakia, J. Souglakos, E.G. Tzortzakic, J. Drositis, G.S. Delides, V. Georgoulias, E.N. Stathopoulos, J. Lung Cancer 57 (2007) 193–200.
[6] D.N. Amin, M.R. Campbell, M.M. Moasser, Semin. Cell. Dev. Biol. 21 (2010) 944–950.
[7] M. Reschke, D. Mihic-Probst, E.H. van der Horst, P. Knyazev, P.J. Wild, M. Hutterer, Clin. Cancer Res. 14 (2008) 5188–5197.
[8] K. Buac, M. Xu, J. Cronin, A.T. Weeraratna, S.M. Hewitt, W.J. Pavan, Pigment Cell Melanoma Res. 22 (2009) 773–784.
[9] M. Soler, F. Mancini, O. Meca-Cortes, L. Sanchez-Cid, N. Rubio, S. Lopez-Fernandez, Int. J. Cancer 125 (2009) 2565–2575.
[10] F. Ciardiello, N. Kim, T. Saeki, R. Dono, M.G. Persico, G.D. Plowman, Proc. Natl. Acad. Sci. USA 88 (1991) 7792–7796.
[11] T. Rajkumar, C.S. Gooden, N.R. Lemoine, W.J. Gullick, C.S. Goden, J. Pathol. 170 (1993) 271–278.
[12] C.A. Maurer, H. Friess, B. Kretschmann, A. Zimmermann, A. Stauffer, H.U. Baer, Hum. Pathol. 29 (1998) 771–777.
[13] P. Kountourakis, K. Pavlakis, A. Psyrri, D. Rontogianni, N. Xiros, E. Patsouris, D. Pectasides, T. Economopoulos, BMC Cancer 6 (46) (2006) 1–9.
[14] S. Kapitanovic, S. Radosevic, N. Slade, M. Kapitanovic, S. Andelinovic, Z. Ferencic, J. Cancer Res. Clin. Oncol. 126 (2000) 205–211.
[15] Z. Suo, J.M. Nesland, Ultrastruct. Pathol. 26 (2002) 125–135.
[16] L.G. Bobrow, R.R. Millis, L.C. Happerfield, W.J. Gullick, Eur. J. Cancer 33 (1997) 1846–1850.
[17] R. Naidul, M. Yadavl, S. Nair, M.K. Kutty, Br. J. Cancer 78 (1998) 1385–1390.
[18] B.J.B. Simpson, J. Weatherill, E.P. Miller, A.M. Lessells, S.P. Langdon, W.R. Miller, Br. J. Cancer 71 (1995) 758–762.
[19] S.O. Addo-Yobo, J. Straessle, A. Anwar, A.M. Donson, B.K. Kleinschmidt, N.K. Foreman, J. Neuropathol. Exp. Neurol. 65 (2006) 769–775.
[20] T.G. Sithanandam, L.M. Anderson, Cancer Gene Ther. 15 (2008) 413–448.
[21] S.H. Lin, Y.C. Lee, M.B. Choueiri, S. Wen, P. Mathew, X. Ye, K.A. Do, N.M. NavoneJ. KimS.M. Tu, L.Y. Yu-Lee, C.J. Logothetis, Clin. Cancer Res. 14 (12) (2008) 3729–3736.
[22] D.N. Poller, I. Spendlove, C. Baker, R. Church, I.O. Ellis, G.D. Plowman, R.J. Mayer, J. Pathol. 168 (1992) 275–280.
[23] M.H. Kraus, W. Issing, T. Miki, N.C. Popescu, S.A. Aaronson, PNAS 23 (1989) 9193–9197.
[24] L. Aurisicchio, E. Marra, L. Luberto, F. Carlomosti, C. De Vitis, A. Noto, Z. Gunes, G. Roscilli, G. Mesiti, R. Mancini, M. Alimandi, G. Ciliberto, J. Cell. Physiol. 227 (2012) 3381–3388.

[25] K.D. Steffensen, M. Waldstrom, R.F. Andersen, D.A. Olsen, U. Jeppesen, H.J. Knudsen, I. Brandslund, A. Jakobsen, Int. J. Oncol. 33 (2008) 195–204.
[26] N.R. Lemoine, D.M. Barnes, D.P. Hollywood, C.M. Hughes, P. Smith, E. Dublin, S. A. Prigent, W.J. Gullick, H.C. Hurst, Br. J. Cancer 66 (1992) 1116–1121.
[27] L. Shaoping, Y. Guan, D. Wang, Y. Du, Anal. Chim. Acta 772 (2013) 26–32.
[28] J.G. Guan, Y.Q. Miao, Q.J. Zhang, J. Biosci. Bioeng. 97 (2004) 4219–4226.
[29] B.P. Marco, Electrochim. Acta 51 (2006) 6217–6229.
[30] E. Valério, L.M. Abrantes, A.S. Viana, Electroanalysis 20 (2008) 2467–2474.
[31] R.G. Nuzzo, D.L. Allara, J. Am. Chem. Soc. 105 (1983) 4481–4483.
[32] D.A. Barrett, G.M. Power, M.A. Hussain, I.D. Pitfield, P.N. Shaw, M.C. Davies, J. Sep. Sci. 28 (5) (2005) 483–491.
[33] L. Li, S. Chen, S. Jiang, J. Biomater. Sci. Polym. Ed. 18 (11) (2007) 1415–1427.
[34] M. Han, D. Ishikawa, T. Honda, E. Ito, M. Hara, Chem. Commun. 46 (2010) 3598–3600.
[35] J. Wen, Z. Tian, J. Ma, J. Phys. Chem. C 117 (2013) 19934–19944.
[36] B. Patil, Y. Kobayashi, S. Fujikawa, T. Okajima, L. Mao, T. Ohsaka, Bioelectrochemistry 95 (2014) 15–22.
[37] D.R.P. Morris, J. Fatisson, A.L.J. Olsson, N. Tufenkji, A.R. Ferro, Sensor Actuators B: Chem. 190 (2014) 851–857.
[38] X. Liu, W.-J. Li, L. Li, Y. Yang, L.-G. Mao, Z. Peng, Sensor Actuators B: Chem. 191 (2014) 408–414.
[39] J.H. Lee, S.H. Cho, H.W. Lim, S.W. Kim, A.A. Busnaina, H.Y. Lee, J.G. Park, Solid State Phenom. 195 (2012) 82–85.
[40] L. Shi, Z. Chu, X. Dong, W. Jin, E. Dempsey, Nanoscale 5 (2013) 10219–10225.
[41] C.M.A. Brett, A.M. Oliveira Brett, Electrochemistry, Principles, Methods, and Applications, Oxford University Press, USA, 1993.
[42] H.A. Kramers, Phys. Z. 30 (1929) 522–523.
[43] R.L. Kronig, J. Opt. Soc. Am. Rev. Sci. Instrum. 12 (1926) 547–557.
[44] W. Ehm, H. Gohr, R. Kaus, B. Roseler, C.A. Schiller, ACH Models Chem. 137 (2000) 145–157.
[45] Q.A. Huang, R. Hui, B. Wang, J. Zhang, Electrochim. Acta 52 (2007) 8144–8164.